International Journal of Refractory Metals & Hard Materials 76 (2018) 33–40

Contents lists available at ScienceDirect

International Journal of Refractory Metals & Hard Materials

journal homepage: www.elsevier.com/locate/IJRMHM

Effects of swaging and annealing on the microstructure and mechanical properties of ZrC dispersion-strengthened tungsten

R. Liu[a], Z.M. Xie[a], X. Yao[a,b], T. Zhang[a,*], X.P. Wang[a], T. Hao[a], Q.F. Fang[a,b,*], C.S. Liu[a]

[a] Key Laboratory of Materials Physics, Institute of Solid State Physics, Chinese Academy of Sciences, Hefei 230031, China
[b] University of Science and Technology of China, Hefei 230026, China

ARTICLE INFO

Keywords:
Tungsten
ZrC
Swaging
Mechanical property
Thermal stability

ABSTRACT

Nano-sized ZrC dispersion strengthened tungsten alloy (W-0.5wt%ZrC) rods with enhanced mechanical properties and superior high-temperature stability were fabricated by high temperature rotary swaging. The effects of swaging and annealing on the microstructure and mechanical properties of W-0.5wt%ZrC alloys were investigated. The as-swaged W-0.5%ZrC rod showed noticeable ductility at 200 °C with a total elongation of 4.2% and a tensile strength of 724 MPa, and at 500 °C the strength remains as high as 547 MPa and the total elongation is 28%. The ductile-to-brittle transition temperature (DBTT) is about 200 °C. The recrystallization start temperature of swaged W-0.5wt%ZrC is about 1500 °C, which is about 300 °C higher than that of rolled pure W. The possible mechanisms for the enhanced mechanical properties and thermal stability were discussed.

1. Introduction

Tungsten is a refractory metal with high melting temperature, high strength, low coefficient of thermal expansion and low vapor pressure, and has been widely used for high-temperature and electric applications. Tungsten has also been considered as one of the most promising candidates for plasma facing materials in future fusion reactors due to its high energy threshold for sputtering, high thermal conductivity, low swelling and low tritium retention [1, 2]. However, in contrast to these excellent properties, the main disadvantage of tungsten material is its brittleness including low-temperature brittleness, recrystallization brittleness and irradiation-induced brittleness [3, 4]. Tungsten with relatively high ductile-to-brittle transition temperature (DBTT) above 400 °C also leads to poor machinability. Besides, the strength of pure tungsten decreases remarkably when temperature rises to above 1000 °C.

A major reason for the low-temperature brittleness of tungsten materials is their sensitivity to some interstitial impurities such as O and N, especially when these impurities segregate at grain boundaries (GBs) leading to poor cohesive strength of GBs [5–7]. Therefore, ductility at low-temperature would be improved if interstitial elements are minimized [2]. For example, H. Kurishita et al. [5] reported that the DBTT decreased drastically from over 420 K to 230 K with the oxygen content decreasing from 870 wt ppm to 160 wt ppm. Therefore, addition of a little Zr could also improve the low-temperature ductility by removal of the atomic oxygen on GBs owing to the Zr element reacting with impurity oxygen and forming stable oxide particles [8, 9]. Refining grains to obtain ultrafine-grained or nano-grained materials by severe plastic deformation could provide abundant GBs that could decrease the average concentration of impurities at GBs [7, 10], and thus is another way to decrease DBTT. However, the microstructure of the ultrafine-grained or nano-grained materials leads to low thermal stability (low recrystallization temperature) due to the large volume fraction of unstable GBs [11, 12]. The dispersion of small amounts of thermal-stable oxide (La_2O_3, Y_2O_3 e. g.) or carbide (TiC, ZrC, TaC, e. g.) particles into tungsten could refine grains and increase the high-temperature strength, recrystallization temperature and creep resistance owing to the effects of pinning dislocations and GBs [4, 13–16]. In the conventional oxide dispersion-strengthened (ODS) tungsten materials however, the oxide particles tend to segregate at GBs and form coarse particles, which cause stress concentration at GBs and lead to intergranular fracture [12]. Among the strengthening phases, ZrC has a much higher melting temperature (3540 °C) as compared with Y_2O_3 and La_2O_3, and ZrC as an oxygen getter could diminish the detrimental influence of oxygen and thus enhance the cohesive strength of GBs [16, 17]. It was reported that ZrC dispersion strengthened W alloys exhibited excellent mechanical properties, such as high strength, high ductility, low DBTT (about 100 °C), as well as enhanced thermal stability and high resistance to thermal shocks [17].

It is well known that the performance and properties of tungsten are closely related to the fabrication route and thermomechanical treatment. Thermomechanical processing such as hot-rolling, forging and

* Corresponding authors at: Key Laboratory of Materials Physics, Institute of Solid State Physics, Chinese Academy of Sciences, Hefei 230031, China.
E-mail addresses: zhangtao@issp.ac.cn (T. Zhang), qffang@issp.ac.cn (Q.F. Fang).

https://doi.org/10.1016/j.ijrmhm.2018.05.018
Received 11 April 2018; Received in revised form 23 May 2018; Accepted 26 May 2018
Available online 30 May 2018
0263-4368/

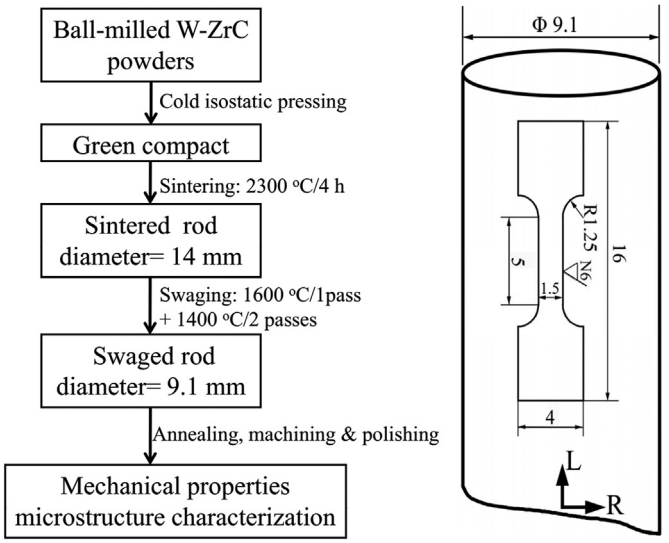

Fig. 1. Schematic diagram of experimental procedures and the tensile test sample cut from the swaged W-0.5ZrC.

swaging has been reported to have a strong influence on the mechanical properties and DBTT of tungsten [9, 18]. In our previous work, W-ZrC alloys have been fabricated through different routes including spark-plasma sintering (SPS) and hot-rolling, and their mechanical properties are significantly different [16, 17]. The hot-rolled W-0.5wt%ZrC exhibited excellent mechanical properties and thermal stability. In this work, W-0.5wt%ZrC rods were fabricated through ball-milling, sintering and high temperature rotary swaging. The effects of swaging and annealing on the microstructure and mechanical properties of W-0.5wt%ZrC rods were investigated.

2. Experimental

2.1. Starting materials and fabrication

W-0.5wt%ZrC alloy (W-0.5ZrC) rods were fabricated using commercial pure W powders (purity > 99.9% trace metals basis, average particle size 500–600 nm) and nano-sized ZrC powders (average particle size ~50 nm, purity > 99%). A schematic diagram of the experimental procedures is plotted in Fig. 1. The powders were ball-milled in a planetary ball mill for 4 h in argon atmosphere with a rotation speed of 240 rpm and ball-to-powder weight ratio of 8:1. Tungsten carbide balls and mortars were used to minimize the impurity contamination. The ball-milled powders were subsequently compacted into a cylindrical rod with a diameter of about 16 mm by cold isostatic pressing and then sintered at 2300 °C for 4 h in flowing dry hydrogen. The diameter of as-sintered W-0.5ZrC rod was about 14 mm. The as-sintered rod was heated at 1600 °C in a hydrogen atmosphere, and swaged into a rod with a diameter of 9.1 mm using a rotary swaging machine. The density of swaged W-0.5ZrC specimens was measured by the Archimedes methods and the relative density was calculated based on the theoretical density of W (19.3 g/cm^3) and ZrC (6.73 g/cm^3).

2.2. Mechanical property test

In order to study the effects of annealing temperature on the mechanical properties and microstructure of the swaged W-0.5ZrC alloys, samples were annealed at different temperatures from 1000 °C to 1800 °C for 1 h in vacuum. The annealed samples were cut and polished for Vickers micro-hardness tests and tensile tests. The micro-hardness tests were carried out at room-temperature (RT) by using a Vickers micro-hardness tester with a load of 200 g and a dwell time of 15 s. For tensile tests, the as-swaged and the annealed W-0.5ZrC samples were cut into dog-bone shaped samples with a cross-section of 1.5×0.75 mm^2 and a gauge length of 5 mm along longitudinal direction (L-direction), as illustrated in Fig. 1. Tensile tests were performed at various temperatures from room-temperature to 500 °C using Instron-5967 machine at a constant displacement speed corresponding to a strain rate of 2×10^{-4} s^{-1}.

2.3. Microstructure characterization

The tungsten samples were polished and etched for metallographic characterization. The recrystallization temperature was determined to be the critical temperature at which tungsten grains grow significantly after holding for 1 h. The fracture surfaces of tensile-tested samples were characterized using a field-emission scanning electron microscope (FE-SEM Sirion200, FEI). The orientation and distribution of tungsten grains of as-swaged W-0.5ZrC in different directions were characterized by electron backscatter diffraction (EBSD, OXFORD NordlysNano) in a FEI Sirion200 SEM. The microstructure of tungsten alloy was characterized by using a JEOL JEM-2000FX transmission electron microscope (TEM). Energy-dispersive X-ray spectroscopy (EDS, INCA) installed in TEM was used for elemental analysis.

3. Results and discussion

3.1. Microstructure of starting materials and swaged samples

Fig. 2 shows the SEM or TEM images of the as-received W powders, ZrC powders and ball-milled W-ZrC powders. The average particle size of W powders is about 600 nm (see Fig. 2a) and some agglomeration in W powders can be found. The TEM image of the ZrC powders after ultrasonic sound treatment in ethanol shows that the average particle size of ZrC powders is about 50 nm (Fig. 2b). After ball-milling, the agglomeration of W particles was alleviated and the ZrC particles were well dispersed in tungsten powders (Fig. 2c). The ball-milled powders were subjected to cold isostatic pressing, high-temperature sintering and swaging, leading to nearly full dense W-0.5ZrC rods with a high relative density of 99.4%.

The EBSD results of the as-swaged W-0.5ZrC in different planes (parallel to and perpendicular to L-direction) and the corresponding inverse pole figure colored map are presented in Fig. 3. The

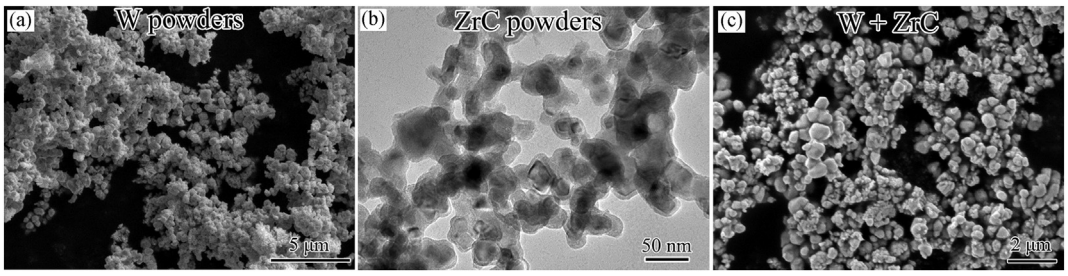

Fig. 2. (a) SEM image of as-received W powders, (b) TEM image of ZrC powders, and (c) SEM image of ball-milled W-0.5ZrC powders.

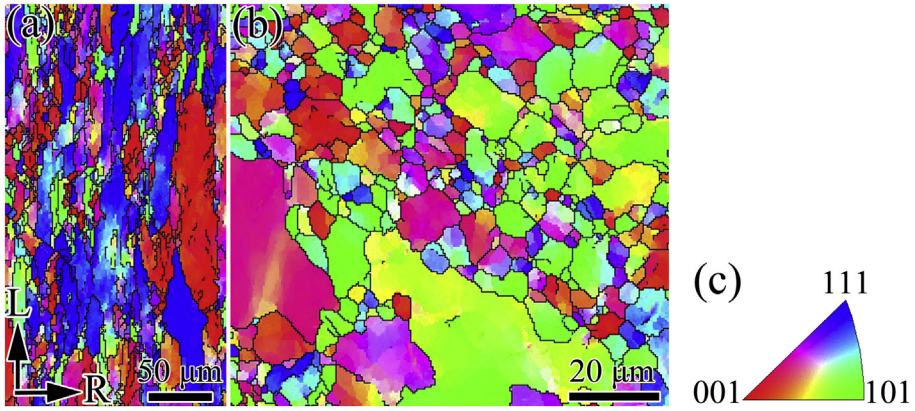

Fig. 3. EBSD images of swaged W-0.5ZrC in the planes (a) parallel to and (b) perpendicular to the longitudinal direction, and (c) inverse pole figure colored map for the samples.

misorientation angle > 10° was adopted to distinguish the GBs. It can be seen that tungsten grains were elongated along the L-direction (Fig. 3a), while the grains in R-direction are nearly equiaxed (Fig. 3b). The average grain size of the as-swaged W-0.5ZrC is about 35 μm in L-direction and 7 μm in radial direction (R-direction), corresponding to an aspect ratio of about 5:1. Several large equiaxed grains were found in plane perpendicular to L-direction (Fig. 3b). The non-uniform grain size of the swaged W-ZrC alloy could be mainly attributed to the different degree of plastic deformation in different parts of the samples during the swaging process. The texture homogeneity of the swaged W-0.5ZrC could be improved by increasing the degree of plastic deformation during swaging process.

3.2. Thermal stability

In order to study the thermal stability of the swaged W-0.5ZrC, the samples were annealed at temperatures from 1000 °C to 1800 °C in vacuum for 1 h. The metallographic images of the as-swaged W-0.5ZrC and the annealed samples are plotted in Fig. 4. It can be seen that the grain growth is not obvious even when the annealing temperature increases to 1500 °C. When the annealing temperature increases from 1600 °C to 1800 °C, the grain size increases significantly, but the grains still maintain elongated shape. These results suggest that the recrystallization start temperature of the swaged W-0.5ZrC is about 1500 °C, which is > 300 °C higher than that of the rolled pure W [19]. It was reported that the recrystallization start temperature of hot-rolled W-0.5ZrC is about 1300 °C and most of the elongated tungsten grains were replaced by larger equiaxed grains after annealing at 1600 °C [20]. These results indicate that the swaged W-0.5ZrC has better thermal stability and has a higher recrystallization temperature than the hot-rolled W-0.5ZrC. It is well known that the materials with fine grains and processed by severe plastic working tends to have a lower recrystallization temperature. Therefore, the higher recrystallization temperature of the swaged W-0.5ZrC is reasonable, because the hot-rolled W-0.5ZrC has much finer grains and the degree of plastic deformation during rolling process is much higher as compared with the swaged one.

The Vickers micro-hardness of the as-swaged W-0.5ZrC in the plane parallel to L-direction is 452 HV, which is slightly lower than that in the plane perpendicular to L-direction (474 HV). Such a difference in hardness can be attributed to the different grain size of the two directions. It is well known that the hardness is intimately linked to the microstructure of materials. Therefore, the recrystallization behavior could be also reflected by the evolution of hardness with annealing temperatures. Fig. 5 shows the Vickers micro-hardness of swaged W-0.5ZrC samples annealed at different temperatures from 1000 °C to 1800 °C. The hardness of the samples does not decrease obviously even at temperature up to 1500 °C. The hardness for the samples annealed at temperatures between 1000 °C and 1500 °C is in the range of 440 HV to 450 HV, which is slightly lower than that of the as-swaged W-0.5ZrC (452 HV). In this temperature range, the residual stress in samples was released while the grain growth is limited. Although the grains begin to grow at 1500 °C (Fig. 4d), the hardness of the sample annealed at 1500 °C just decrease a little. When the annealing temperature increases to 1600 °C and 1800 °C, the hardness decreases remarkably to about 420 HV and 400 HV, respectively. The recrystallization start temperature could be estimated as 1500 °C, which is about 200 °C and 300 °C higher than those of the rolled W-0.5ZrC and the rolled pure W, respectively [19].

3.3. Effects of annealing and swaging on the tensile properties

The engineering stress–strain curves of the as-swaged W-0.5ZrC and the W-0.5ZrC samples annealed at 1300 °C, 1500 °C and 1600 °C are presented in Fig. 6 without correction of machine-compliance. In order to more clearly present the evolution of tensile properties with annealing temperature, the ultimate tensile strength (UTS) and total elongation (TE) of the as-swaged and the annealed W-0.5ZrC were plotted in Fig. 7a-b. The as-swaged W-0.5ZrC is brittle at 150 °C and exhibited obvious ductility at 200 °C with a TE of 4.2% and the UTS is 724 MPa. This results suggests that the DBTT of the as-swaged W-0.5ZrC is about 200 °C, which is much lower than that of the rolled pure W [19]. With test temperature increasing to 300 °C, the UTS decreases to 631 MPa while the TE increases significantly to 19%. At 500 °C, the UTS of the as-swaged W-0.5ZrC is as high as 547 MPa and the TE is about 28%. For the sample annealed at 1300 °C for 1 h (A1300 sample), the strength is comparable with the as-swaged W-0.5ZrC, but the ductility was obviously improved especially at low temperatures. At 200 °C, the TE of A1300 sample reaches 9%, which is much higher than that of the as-swaged ones (4.2%). At a higher temperature of 500 °C, the strength of A1300 sample is still as high as 533 MPa and the TE is 28.4%. After annealing at 1500 °C, the UTS of the swaged W-0.5ZrC at 500 °C decreases to 491 MPa while the TE values at temperatures between 300 °C and 500 °C are always higher than 24%. With the elevating annealing temperature to 1600 °C, the strength decreases drastically. Nevertheless, the strength of the swaged W-0.5ZrC annealed at 1600 °C (A1600) is still very high, noting that its UTS at 500 °C is 407 MPa, which is about 35% higher than that of hot-rolled W-0.5ZrC (~300 MPa) [20]. The swaged W-0.5ZrC has higher thermal stability and better ability to withstand recrystallization than the hot-rolled W-0.5ZrC [20]. The A1600 samples have excellent ductility at temperatures above 300 °C and the TE at 500 °C is as high as 35%. As compared with the as-swaged W-0.5ZrC, the A1600 samples showed lower strength but much better ductility, which could be attributed to

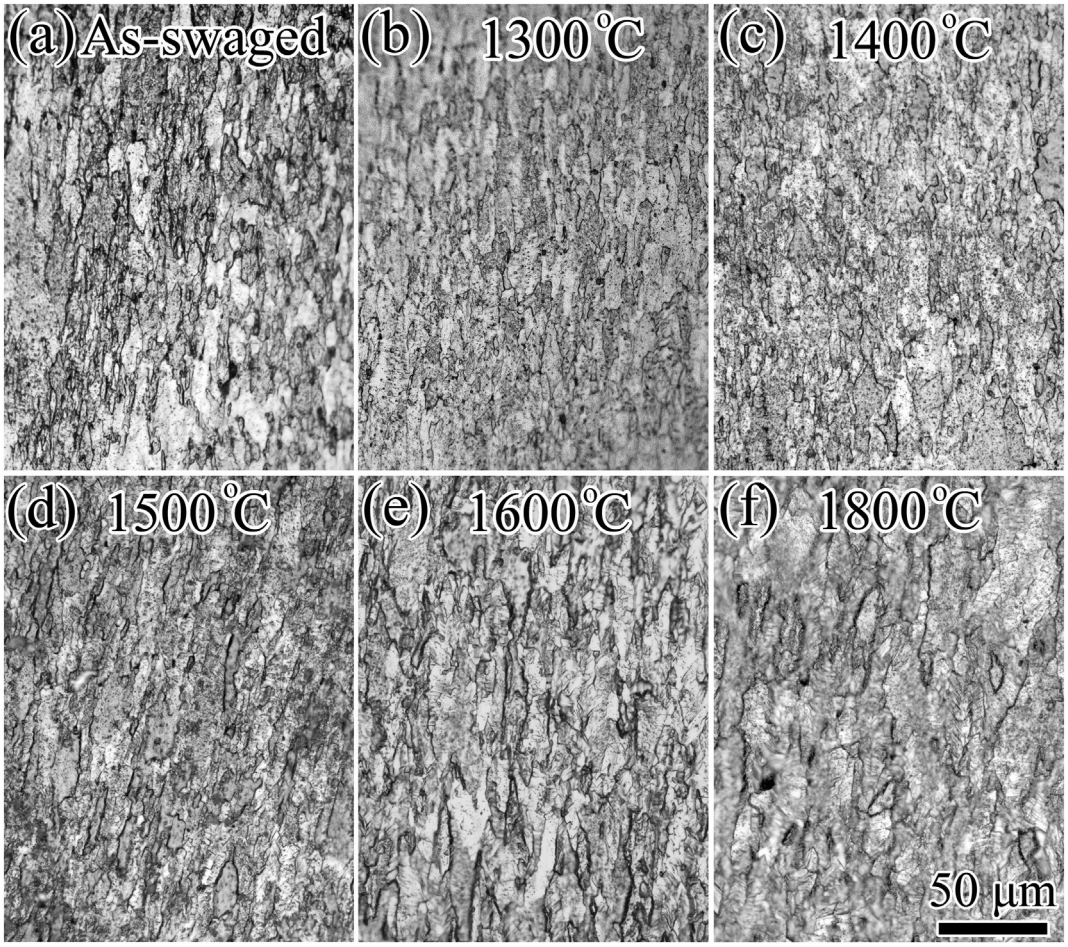

Fig. 4. Metallographic images of (a) as-swaged W-0.5ZrC, and (b-f) W-0.5ZrC samples annealed at 1300 °C, 1400 °C, 1500 °C, 1600 °C and 1800 °C.

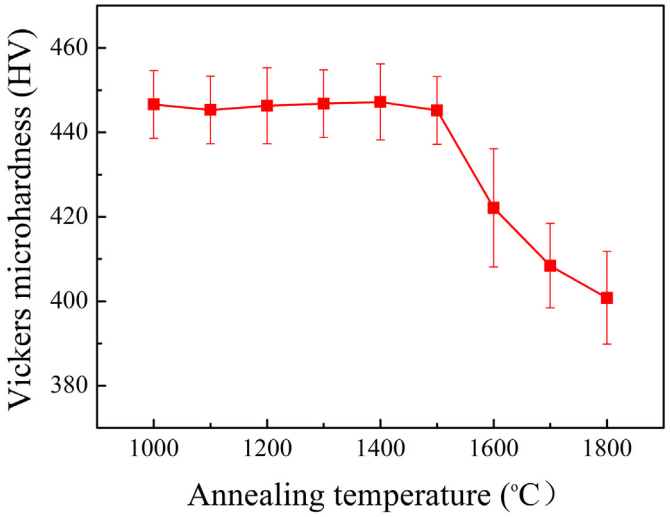

Fig. 5. Vickers micro-hardness of the swaged W-0.5ZrC versus annealing temperatures (for 1 h).

dislocation annihilation and grain growth during high temperature annealing. In the as-swaged W-0.5ZrC, the high density of defects like dislocations that tends to pile up at the GBs could cause stress concentration and become possible sites of cracks initiation. These could explain that the as-swaged W-0.5ZrC have fine grains and high strength, but lower ductility. After high temperature annealing, the density of dislocations decreases considerably and the effects of strain hardening are eliminated. The large grain size and decreased dislocation density result in a low strength. The recrystallization process consists of the nucleation of a strain-free region whose boundary can transform the strained matrix into strain-free grains as it moves. The strain-free grains could provide more rooms to accommodate dislocations during the subsequent tensile tests. Therefore, the W-0.5ZrC annealed at 1600 °C exhibits much better ductility (tensile elongation) as compared with the as-swaged ones.

The recrystallization of W materials often leads to embrittlement. According to the Vickers micro-hardness results (Fig. 5), recrystallization occurred when the samples were annealed at 1600 °C. However, the DBTT of the swaged W-0.5ZrC was not increased even after annealing at a high temperature of 1600 °C. This result suggests that the recrystallization embrittlement of W materials could be alleviated by the addition of small amount of ZrC. Similar results were found in the hot-rolled W-0.5ZrC [20]. During the recrystallization and/or grain growth process, the GBs collect impurities such as oxygen in the region swept through, leading to increased oxygen concentration at GBs. It is known that a major reason for the low-temperature brittleness of W materials is their sensitivity to some interstitial impurities (such as O, N), especially when they segregate at GBs. The increased concentration of detrimental oxygen at GBs would decrease the cohesive strength of GBs, and thus cause low-temperature intergranular fracture (recrystallization embrittlement). While in the W-0.5ZrC alloys, ZrC as an oxygen getter could react with impurity oxygen to form stable oxide particles during sintering process, which would reduce the detrimental oxygen concentration at GBs and thus alleviate the recrystallization embrittlement [20].

To evaluate the effects of swaging on the tensile properties, the UTS

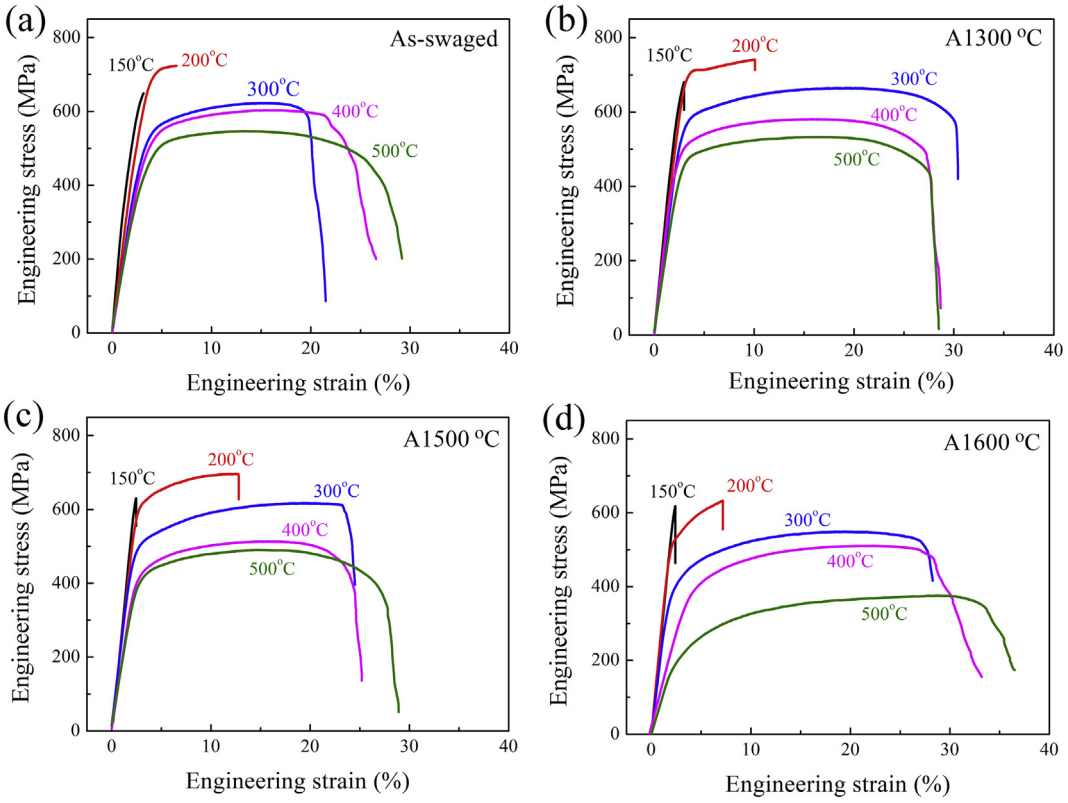

Fig. 6. Tensile engineering stress-strain curves of (a) swaged W-0.5ZrC and (b-d) W-0.5ZrC after annealing at 1300 °C, 1500 °C and 1600 °C in vacuum for 1 h.

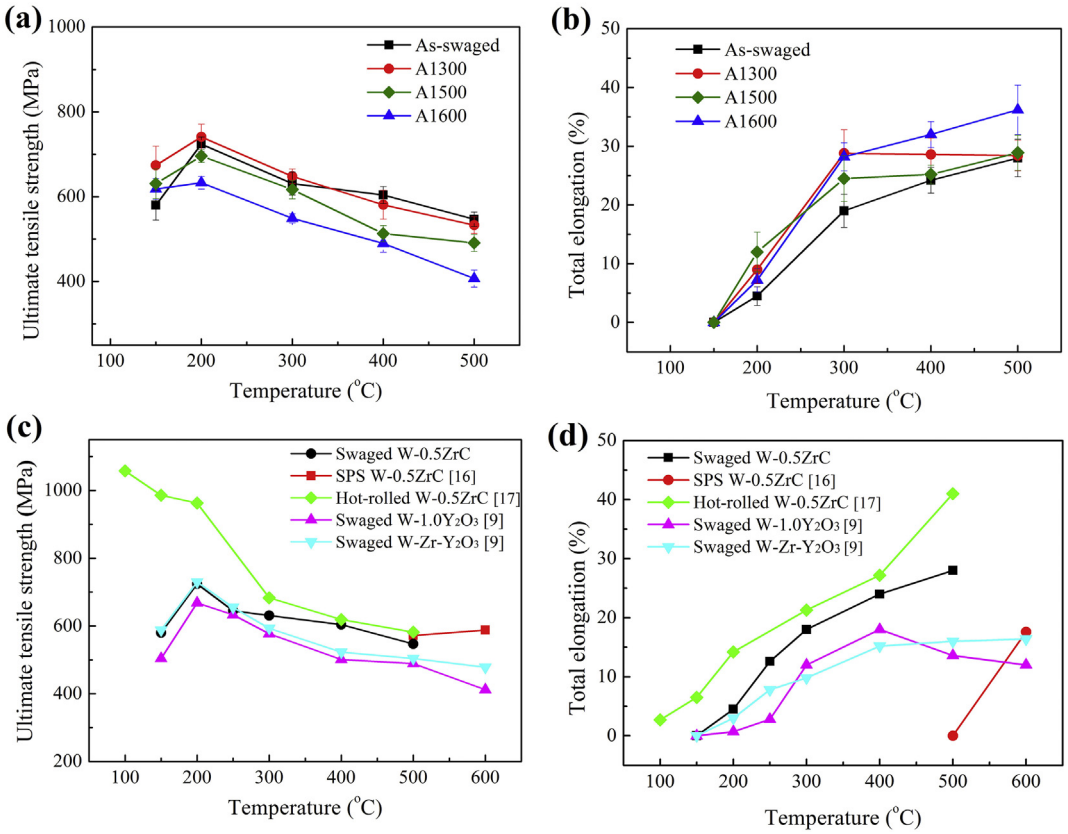

Fig. 7. Effects of annealing temperature on the (a) UTS and (b) TE of swaged W-0.5ZrC, and the (c) UTS and (d) TE of swaged W-0.5ZrC in comparison with SPS W-0.5ZrC, hot-rolled W-0.5ZrC, swaged W-1.0Y_2O_3 and swaged W-0.2Zr-1.0Y_2O_3.

and TE of W-0.5ZrC alloys fabricated by different methods including swaging, SPS and hot-rolling were shown in Fig. 7c-d. As compared with the SPS W-0.5ZrC, the swaged W-0.5ZrC showed significant enhancement in ductility especially at low-temperatures. The SPS W-0.5ZrC is brittle even at a high temperature of 500 °C, while the swaged W-0.5ZrC and hot-rolled W-0.5ZrC show ductility at 200 °C and 100 °C, respectively [16, 17]. The strength of the swaged W-0.5ZrC at 500 °C is comparable to that of the SPS W-0.5ZrC, although the grain size of the swaged W-0.5ZrC (35 μm in L-direction and 7 μm in R-direction) is much larger than that of SPS W-0.5ZrC (4.2 μm). According to the Hall-Petch equation, the strength of the SPS W-0.5ZrC with fine grains should be much higher. However, the relative density of the SPS W-0.5ZrC (97.5%) is lower than that of the swaged W-0.5ZrC (99.4%). The higher porosity of SPS W-0.5ZrC would undoubtedly lead to lower strength. Besides, the dominant intergranular fracture in SPS W-0.5ZrC at low temperature implies the low cohesive strength of grain boundaries [16]. While in the swaged W-0.5ZrC, the cohesive strength of grain boundaries could be enhanced by hot swaging. Therefore, due to higher relative density and enhanced cohesive strength of grain boundaries, the strength of the swaged W-0.5ZrC is comparable to that of the SPS W-0.5ZrC, although the grain size of SPS W-0.5ZrC is much smaller. These results indicate that the thermomechanical processing such as swaging and rolling have a strong influence on the mechanical properties of tungsten. Both the strength and ductility of the swaged W-0.5ZrC are lower than those of the hot-rolled W-0.5ZrC at temperatures from RT to 500 °C [17]. The lower strength of the swaged W-0.5ZrC could be mainly attributed to its larger grain size (about 35 μm in length and 7 μm in width), which is much larger than that of the hot-rolled W-0.5ZrC. For the hot-rolled W-0.5ZrC, the lower sintering temperature and the larger plastic deformation during hot-working processes leads to fine tungsten grains [17]. The fine grain size and large plastic deformation are also responsible for the lower recystallization temperature of the hot-rolled W-0.5ZrC, because the large amount GBs and higher storage energy in materials tends to decrease the thermal stability.

The dispersion of thermal stable oxide or carbide fine particles into tungsten is very effective in improving the strength and high temperature properties. In our previous work, the UTS and TE of swaged W-1.0Y_2O_3 and swaged W-0.2Zr-1.0Y_2O_3 fabricated by a similar route were also presented in Fig. 7c-d for comparison [9, 21]. It can be seen that the swaged W-0.5ZrC showed both higher strength and ductility than the swaged W-1.0Y_2O_3 and W-0.2Zr-1.0Y_2O_3. The lower strength and ductility could be attributed to the formation and segregation of coarse oxide particles at GBs in swaged W-1.0Y_2O_3 and W-0.2Zr-1.0Y_2O_3 during high temperature sintering. For example, in the swaged W-1.0Y_2O_3 alloys reported in ref. [9, 21], many Y_2O_3 particles segregate at GBs and grow into coarse particles after high temperature sintering, although nano-sized Y_2O_3 particles (average particle size ~ 50 nm) were used as starting materials. The coarse Y_2O_3 particles at GBs would not only cause stress-concentration and decrease the ductility, but also reduce the strengthening effects due to the reduced number of Y_2O_3 particles in tungsten. The swaged W-0.2Zr-1.0Y_2O_3 exhibited enhanced strength and ductility as compared with the swaged W-1.0Y_2O_3, because the addition of small amount of Zr could enhance the cohesive strength of GBs and ductility by reacting with impurity oxygen to form stable oxide particles while the dispersion of Y_2O_3 could improve the strength by pinning dislocations [9]. Nevertheless, the strength and ductility of the swaged W-0.2Zr-1.0Y_2O_3 are still lower than those of the swaged W-0.5ZrC. This could be attributed to the different size and distribution of particles in the two materials.

3.4. Fracture morphology and TEM observation

Fig. 8 shows the SEM images from the fracture surfaces of the as-swaged W-0.5ZrC specimens tensile-tested at different temperatures and the intergranular fracture zones are indicated by curves. For the specimen tested at RT and 150 °C, mixed transgranular and intergranular mode fracture can be seen (Fig. 8a), and the area fraction of intergranular fracture is very low. At 200 °C, the fracture morphology of the swaged W-0.5ZrC is dominated by transgranular mode, as shown in Fig. 8c. As compared with the SPSed W-ZrC samples [16], the low area fraction of intergranular fracture in the swaged W-0.5ZrC at relatively low temperatures suggests that the cohesion strength of GBs has been effectively enhanced by hot swaging. At 300 °C, the fracture surface after tensile testing is transgranular ductile dimple mode and the plastic deformation of tungsten grains can be clearly seen (Fig. 8d). This is consistent with the tensile test results that the swaged W-0.5ZrC exhibits good ductility at 300 °C with a TE of about 20%.

The microstructure of the swaged W-0.5ZrC was characterized by TEM (Fig. 9a-c). It can be seen that most of the particles were nanoscale and homogeneously dispersed in tungsten grain interior. The particles in W-0.5ZrC maintain nanoscale although the materials were sintered at a high temperature of 2300 °C for 4 h. This result shows the excellent dimensional stability of ZrC in tungsten. The intragranular nano-sized particles could generate, pin down and accumulate dislocations in the grains, as indicated by solid arrows in Fig. 9c. The pinning and accumulation of dislocations in grains interior could increase the strength and ductility, as reported in ref. [7]. The size distribution of intragranular and intergranular particles in swaged W-0.5ZrC were presented in Fig. 10a-b. The particles in tungsten grain interior are nearly spherical with an average size of about 39 nm and > 90% particles are smaller than 70 nm. For the intergranular particles, the size is in the range of 5–270 nm with a larger average size of 82 nm, and the fraction of the intergranular particles is < 5%. These fine particles impose a strong resistance to GBs migration and could pin GBs by the Zener mechanism [22, 23]. The particles pinning GBs (as indicated by hollow arrows in Fig. 9 b-c) could refine grains and improve the strength and high temperature stability. It is well known that the strength could be effectively enhanced by the dispersion of second-phases, however, the ductility remains inadequate for many dispersion-strengthened materials [7]. An important reason for the low ductility is that the large second-phase particles tend to distribute at GBs and cause stress concentration, leading to intergranular fracture [7, 12]. For the swaged W-0.5ZrC, the stress-concentration and cracks initiations at GBs could be alleviated due to the small size and low fraction of intergranular particles. The large fraction of second phase particles in tungsten grain interior could be attributed to the coherent interfaces between ZrC particles and W that provides high particle-matrix cohesion strength [17]. During the high-temperature sintering and swaging process, the initial sub-micron W particles grow into large grains, while the ZrC particles adhering to W particles were distributed into W grains interior. The EDS analysis indicate that W, Zr, C and/or O signals were detected in particles near or at GBs, while W, Zr and C signals were detected in most intragranular particles. Fig. 9d shows the HRTEM image of several particles near GBs. The measured interplanar distances of the two particles are 0.262 nm and 0.289 nm, which are close to the values of monoclinic ZrO_2 (002) and (111) from the PDF card (reference code: 00–036-0420, 0.262 nm for (002) and 0.284 nm for (111)) considering measurement error, respectively. These results suggest that ZrC particle could react with the oxygen in tungsten to form Zr-C-O or ZrO_2 particles. As a result, the detrimental effects of interstitial oxygen impurity on GBs would be alleviated, and the GBs cohesion strength and low-temperature ductility of W-ZrC would be effectively improved. In addition, the coherent or semi-coherent interfaces between ZrC particles and tungsten matrix, as reported in ref. [17], are also beneficial to diminishing the stress concentration on W/ZrC interface and improve the mechanical properties. The nano-sized ZrC in W-0.5ZrC alloys could enhance the grains by pinning dislocations, enhance GBs by depleting oxygen impurity and pinning GBs. All of these aspects lead to enhanced strength, ductility and thermal stability.

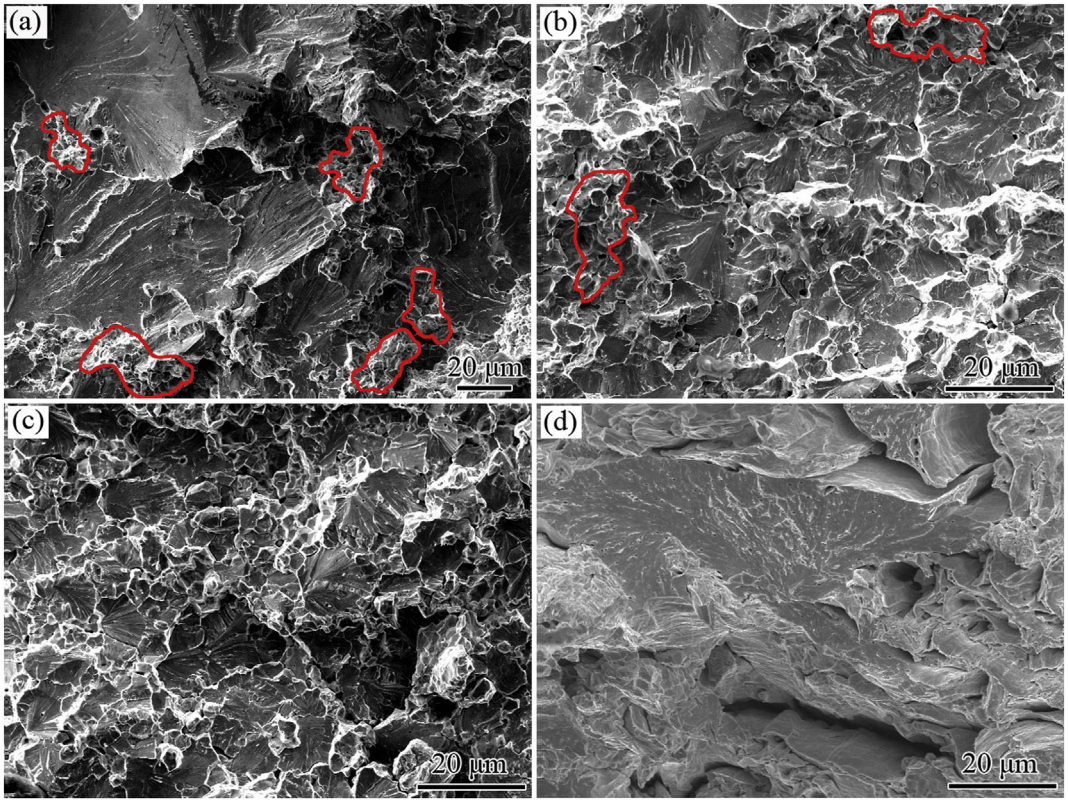

Fig. 8. SEM images of fracture surfaces of the swaged W-0.5ZrC tensile-tested at (a) RT, (b) 150 °C, (c) 200 °C, and (d) 300 °C.

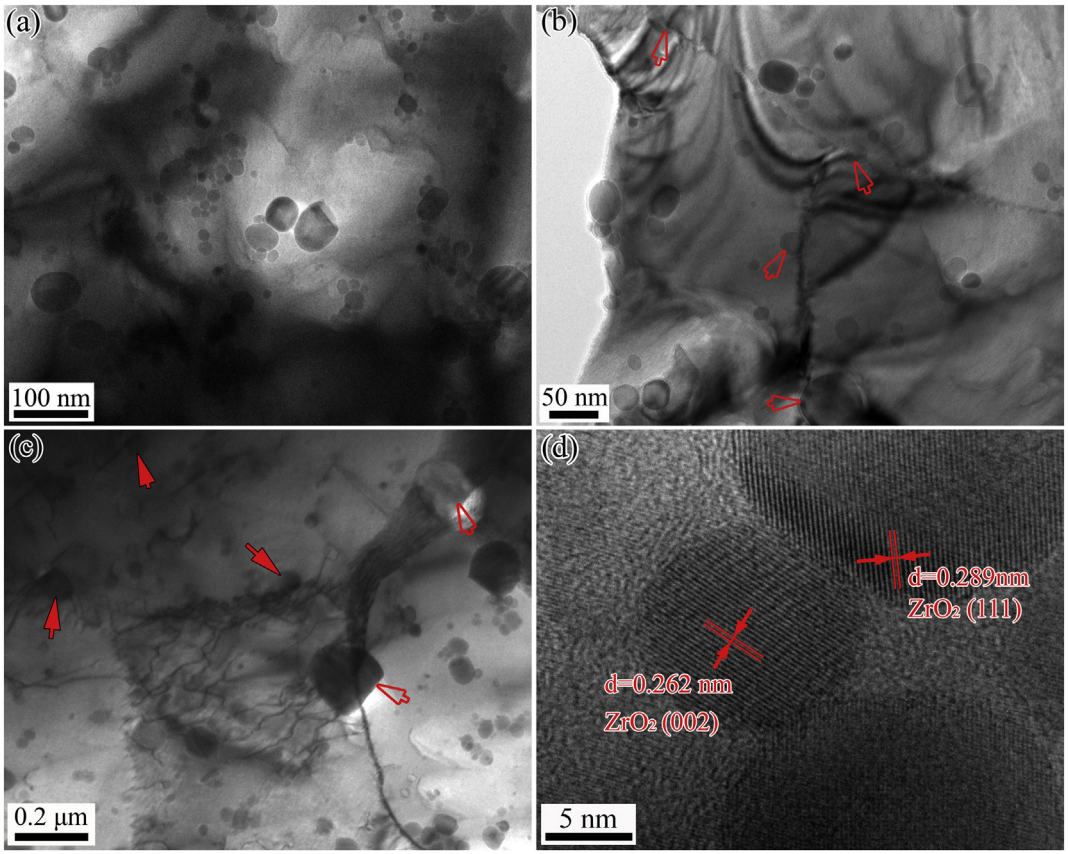

Fig. 9. TEM images of the swaged W-0.5ZrC showing (a) particles in tungsten grains interior, (b) nano-sized particles at GBs indicated by hollow arrows, (c) intragranular particles pinning dislocations (indicated by solid arrows) and some large particles at GBs (indicated by hollow arrows), and (d) HRTEM image of some ZrO_2 particles near GBs.

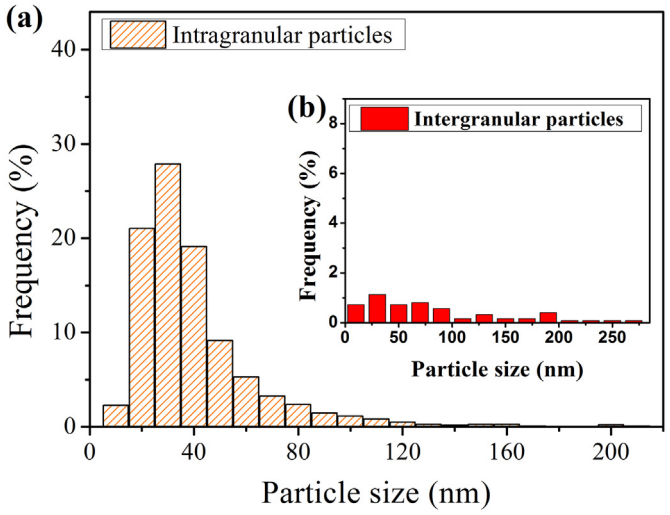

Fig. 10. Particle size distribution of (a) intragranular and (b) intergranular particles in the swaged W-0.5ZrC.

4. Conclusions

Nano-sized ZrC dispersion strengthened tungsten (W-0.5%ZrC) alloy rods with enhanced strength and ductility were fabricated by high temperature rotary swaging. The swaged W-0.5wt%ZrC showed significant enhancement in low temperature ductility as compared with SPS W-0.5ZrC and exhibited a relatively low DBTT of about 200 °C. The swaged W-0.5ZrC also exhibited superior strength and ductility as compared with the swaged W-1.0Y_2O_3 and swaged W-0.2Zr-1.0Y_2O_3. In the swaged W-0.5ZrC, the ZrC particles are nanoscale and most of them were distributed in tungsten grain interior. These intragranular nano-sized particles could improve the strength and simultaneously enhance the ductility by pinning and accumulating dislocations without causing stress concentration at GBs. While in the swaged W-1.0Y_2O_3 and swaged W-0.2Zr-1.0Y_2O_3, larger oxide particles segregating at GBs tend to cause stress concentration, initiate micro-cracks and lead to intergranular fracture. Meanwhile, the ZrC particles could alleviate the detrimental effects of oxygen on GBs by reacting with oxygen to form stable oxide particles. The depletion of oxygen at GBs would undoubtedly enhance the cohesion strength of GBs and thus improve the ductility.

Although the strength and ductility of the swaged W-0.5ZrC are lower than those of hot-rolled W-0.5ZrC, the swaged W-0.5ZrC shows a better thermal stability than the hot-rolled ones. The higher thermal stability of the swaged W-0.5ZrC could be attributed to the larger grain size and lower degree of deformation during hot working. The recrystallization start temperature of the swaged W-0.5ZrC is about 1500 °C, which is about 200 °C and 300 °C higher than those of the hot-rolled W-0.5ZrC and pure W, respectively. The DBTT of the swaged W-0.5ZrC was not increased even after annealing at a high temperature of 1600 °C, suggesting that the recrystallization embrittlement of W could be inhibited by addition of small amount of ZrC. This could be attributed to the fact that ZrC could capture impurity oxygen to form stable particles, which could decrease the oxygen concentration at GBs and alleviate the recrystallization embrittlement.

Acknowledgements

This work was finantially supported by the National Magnetic Confinement Fusion Program of China (Grant No. 2015GB112000); the National Key Research and Development Program of China (Grant No. 2017YFA0402800); and the National Natural Science Foundation of China (Grant Nos. 51671184, 11475216, 11575231, 51771184, 11575241).

References

[1] P. Norajitra, L.V. Boccaccini, A. Gervash, R. Giniyatulin, N. Holstein, T. Ihli, G. Janeschitz, W. Krauss, R. Kruessmann, V. Kuznetsov, A. Makhankov, I. Mazul, A. Moeslang, I. Ovchinnikov, M. Rieth, B. Zeep, Development of a helium-cooled divertor: material choice and technological studies, J. Nucl. Mater. 367 (2007) 1416–1421.
[2] J. Knaster, A. Moeslang, T. Muroga, Materials research for fusion, Nat. Phys. 12 (2016) 424–434.
[3] H. Kurishita, Y. Amano, S. Kobayashi, K. Nakai, H. Arakawa, Y. Hiraoka, T. Takida, K. Takebe, H. Matsui, Development of ultra-fine grained W-TiC and their mechanical properties for fusion applications, J. Nucl. Mater. 367 (2007) 1453–1457.
[4] H. Kurishita, S. Kobayashi, K. Nakai, T. Ogawa, A. Hasegawa, K. Abe, H. Arakawa, S. Matsuo, T. Takida, K. Takebe, M. Kawai, N. Yoshida, Development of ultra-fine grained W-(0.25-0.8)wt%TiC and its superior resistance to neutron and 3 MeV He-ion irradiations, J. Nucl. Mater. 377 (2008) 34–40.
[5] H. Kurishita, S. Matsuo, H. Arakawa, T. Sakamoto, S. Kobayashi, K. Nakai, H. Okano, H. Watanabe, N. Yoshida, Y. Torikai, Y. Hatano, T. Takida, M. Kato, A. Ikegaya, Y. Ueda, M. Hatakeyama, T. Shikama, Current status of nanostructured tungsten-based materials development, Phys. Scr. T159 (2014) 014032.
[6] R. Liu, Z.M. Xie, T. Hao, Y. Zhou, X.P. Wang, Q.F. Fang, C.S. Liu, Fabricating high performance tungsten alloys through zirconium micro-alloying and nano-sized yttria dispersion strengthening, J. Nucl. Mater. 451 (2014) 35–39.
[7] G. Liu, G.J. Zhang, F. Jiang, X.D. Ding, Y.J. Sun, J. Sun, E. Ma, Nanostructured high-strength molybdenum alloys with unprecedented tensile ductility, Nat. Mater. 12 (2013) 344–350.
[8] Z.M. Xie, R. Liu, Q.F. Fang, Y. Zhou, X.P. Wang, C.S. Liu, Spark plasma sintering and mechanical properties of zirconium micro-alloyed tungsten, J. Nucl. Mater. 444 (2014) 175–180.
[9] R. Liu, Z.M. Xie, T. Zhang, Q.F. Fang, X.P. Wang, T. Hao, C.S. Liu, Y. Dai, Mechanical properties and microstructures of W-1%Y2O3 microalloyed with Zr, Mater. Sci. Eng. A 660 (2016) 19–23.
[10] L.J. Kecskes, K.C. Cho, R.J. Dowding, B.E. Schuster, R.Z. Valiev, Q. Wei, Grain size engineering of bcc refractory metals: top-down and bottom-up - application to tungsten, Mater. Sci. Eng. A 467 (2007) 33–43.
[11] R. Liu, Y. Zhou, T. Hao, T. Zhang, X.P. Wang, C.S. Liu, Q.F. Fang, Microwave synthesis and properties of fine-grained oxides dispersion strengthened tungsten, J. Nucl. Mater. 424 (2012) 171–175.
[12] R. Liu, Z.M. Xie, Q.F. Fang, T. Zhang, X.P. Wang, T. Hao, C.S. Liu, Y. Dai, Nanostructured yttria dispersion-strengthened tungsten synthesized by sol-gel method, J. Alloys Compd. 657 (2016) 73–80.
[13] M.A. Yar, S. Wahlberg, H. Bergqivist, H.G. Salem, M. Johnsson, M. Muhammed, Spark plasma sintering of tungsten-yttrium oxide composites from chemically synthesized nanopowders and microstructural characterization, J. Nucl. Mater. 412 (2011) 227–232.
[14] A. Munoz, M.A. Monge, B. Savoini, M.E. Rabanal, G. Garces, R. Pareja, La2O3-reinforced W and W-V alloys produced by hot isostatic pressing, J. Nucl. Mater. 417 (2011) 508–511.
[15] I. Wesemann, W. Spielmann, P. Heel, A. Hoffmann, Fracture strength and microstructure of ODS tungsten alloys, Int. J. Refract. Met. Hard Mater. 28 (2010) 687–691.
[16] Z.M. Xie, R. Liu, Q.F. Fang, T. Zhang, Y. Jiang, X.P. Wang, C.S. Liu, Microstructure and mechanical properties of nano-size zirconium carbide dispersion strengthened tungsten alloys fabricated by spark plasma sintering method, Plasma Sci. Technol. 17 (2015) 1066–1071.
[17] Z.M. Xie, R. Liu, S. Miao, X.D. Yang, T. Zhang, X.P. Wang, Q.F. Fang, C.S. Liu, G.N. Luo, Y.Y. Lian, X. Liu, Extraordinary high ductility/strength of the interface designed bulk W-ZrC alloy plate at relatively low temperature, Sci. Rep. 5 (2015) 16014.
[18] T.L. Shen, Y. Dai, Y. Lee, Microstructure and tensile properties of tungsten at elevated temperatures, J. Nucl. Mater. 468 (2016) 348–354.
[19] H.W. Deng, Z.M. Xie, Y.K. Wang, R. Liu, T. Zhang, T. Hao, X.P. Wang, Q.F. Fang, C.S. Liu, Mechanical properties and thermal stability of pure W and W-0.5 wt%ZrC alloy manufactured with the same technology, Mater. Sci. Eng. A 715 (2018) 117–125.
[20] Z.M. Xie, S. Miao, R. Liu, L.F. Zeng, T. Zhang, Q.F. Fang, C.S. Liu, X.P. Wang, Y.Y. Lian, X. Liu, L.H. Cai, Recrystallization and thermal shock fatigue resistance of nanoscale ZrC dispersion strengthened W alloys as plasma-facing components in fusion devices, J. Nucl. Mater. 496 (2017) 41–53.
[21] Z.M. Xie, R. Liu, S. Miao, T. Zhang, X.P. Wang, Q.F. Fang, C.S. Liu, G.N. Luo, Effect of high temperature swaging and annealing on the mechanical properties and thermal conductivity of W-Y2O3, J. Nucl. Mater. 464 (2015) 193–199.
[22] K.A. Darling, M.A. Tschopp, R.K. Guduru, W.H. Yin, Q. Wei, L.J. Kecskes, Microstructure and mechanical properties of bulk nanostructured Cu-Ta alloys consolidated by equal channel angular extrusion, Acta Mater. 76 (2014) 168–185.
[23] K.A. Darling, E.L. Huskins, B.E. Schuster, Q. Wei, L.J. Kecskes, Mechanical properties of a high strength Cu-Ta composite at elevated temperature, Mater. Sci. Eng. A 638 (2015) 322–328.